AIAA JOURNAL
Vol. 41, No. 2, February 2003

Method to Improve the Accuracy of Straight-Segment Representation of Helical Vortices

D. H. Wood*
University of Newcastle, Callaghan, New South Wales 2308, Australia

The errors arising from the computational representation of a helical vortex by straight segments, particularly at the small values of pitch that are typical of the wakes of hovering rotors and wind turbines, are considered. For a helix of constant pitch and radius, as in the far wake, the main error in calculating the velocity at a control point of the same radius arises from the pairs of "aligned segments," whose junction is in line with the control point. The aligned segments are those closest to the control point; for each M segments per revolution of the helix, there is one pair of aligned segments. They are particularly important at small pitch because of their proximity to the control point. An approximate analytic expression is derived for the velocity due to the section of the helix represented by the aligned segments. Its use is shown to improve significantly the accuracy of the induced velocity for the moderate values of M that are used in many calculations. For a vortex of changing radius, typical of the near wake, the aligned segments are also crucial. Replacing them by an extension of the analytic approximation also leads to a significant improvement in the accuracy of the induced velocity at moderate values of M. Calculations of the expanding wake of a three-bladed wind turbine are used to compare the improvement in accuracy at moderate M to that obtained by increasing M without replacement. Replacement caused a much smaller increase in execution time per iteration.

Nomenclature

a	=	vortex core radius
a_0, a_1, a_2	=	constants in Eq. (14)
b_0, b_1, b_2	=	constants in Eq. (14)
F_1, F_2, F_3	=	functions defined in the Appendix
k	=	index of junction of aligned segments
L	=	length of vortex segment
M	=	number of straight segments per revolution of the helix
N	=	number of helical vortices and blades
p	=	vortex pitch
R	=	helix radius
r	=	distance
U	=	x-direction velocity
U_b	=	binormal velocity
V	=	y-direction velocity
W	=	z-direction velocity
$W(p)$	=	function introduced in Eq. (7)
$W(\alpha, p)$	=	function introduced in Eq. (1)
x, y, z	=	coordinate directions defined in Fig. 1
α	=	azimuthal displacement of vortex
β	=	normalized vortex angle
Γ	=	circulation in vortex
ε	=	cutoff parameter
θ	=	vortex angle
θ'	=	vortex angle measured from the junction of a pair of aligned segments

Subscripts

a	=	start of vortex segment
b	=	end of vortex segment
p	=	control point
s	=	value for vortex segment
0	=	junction of aligned pair of vortex segments

Received 23 April 2002; revision received 9 September 2002; accepted for publication 14 September 2002.

*Associate Professor, Discipline of Mechanical Engineering, School of Engineering; David.Wood@newcastle.edu.au.

Introduction

HELICAL vortices occur in the wakes of helicopter rotors, propellers, and wind turbines and can have a significant effect on the flow through the blades. If the inflow is steady and parallel to the axis of rotation, then the helices in the far wake have constant pitch and radius. This simple case has been the subject of considerable recent attention, for example, Refs. 1–4, which has resulted in a good understanding of the self-induced velocity and its variation with vortex pitch p. The main result is that the self-induced binormal velocity at small p, less than about 0.2 when normalized by the vortex radius, has a leading term proportional to p^{-1} due to the proximity of successive turns of the helix. (Note that the binormal velocity is orthogonal to the tangential and normal velocities; for a helix of constant pitch and radius, the normal velocity is in the radial direction. When, in addition, the pitch is small, the binormal direction is nearly the x direction in Fig. 1.) This term is usually significantly larger than the logarithmic term that arises for all curved vortices and is, for example, the main component of the velocity of a vortex ring. Wood and Boersma[4] demonstrated that most operational wind turbines have $p \approx 0.05$ in the far wake and quoted $p = 0.053$ in the far wake of the hovering rotor experiment of Leishman et al.[5] Furthermore, $p^{-1} \to \infty$ as $\downarrow 0$, so that the vortex ring can not be considered as a special case of a helix in this context. The vortex ring, whose velocity field is well known, is not, therefore, a sufficient test case for the development of computational representations of helical vortices.

Perhaps the simplest, and most common, computational representation of helical vortices is by the straight segments shown graphically in Fig. 1 for a constant radius helix with $p = 0.05$. Each revolution of the helix contains M segments, so that the increment in the vortex angle θ measured from the positive y axis in the direction of the helix in Fig. 1, is $2\pi/M$ per segment. $M = 6$ in Fig. 1. In a typical aerodynamic calculation, it would be necessary to compute the three velocity components at some point on each straight segment. The accuracy of the straight-segment approximation has been tested by Bliss et al.[6] and Bhagwat and Leishman,[7] among others, by comparison with the velocity field of a vortex ring. It was shown that the order of accuracy of the approximation is M^{-2}. Bliss et al.[6] developed a curved vortex element with a typical accuracy of M^{-4}, but its use involves significant extra computation. Bhagwat

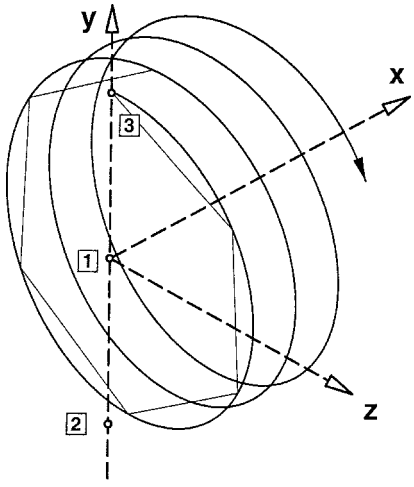

Fig. 1a Helical vortex by straight segments; the helix has constant radius and pitch, $p = 0.05$, and $M = 6$.

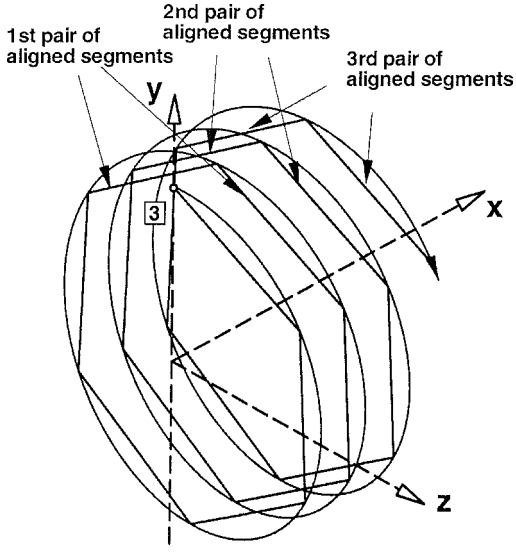

Fig. 1b First three pairs of aligned segments for case 3.

and Leishman[7] showed that the logarithmic term due to curvature, which obviously cannot be captured by straight segments, can easily and accurately be added.

The first use of the recent findings on helical vortices to investigate the accuracy of the straight-segment approximation was by Wood and Li.[8] They confirmed the M^{-2} accuracy for a control point well away from the vortex (their case 1) and then considered two additional control points (cases 2 and 3) at the vortex radius. Case 2 was displaced by 180 deg from the beginning of the helix. Its location would be the origin of the second helical vortex for a two-bladed rotor. Case 3 was on the vortex, giving the self-induced velocity. All three control points are shown in Fig. 1a. Bliss et al.[6] found that the induced velocity calculations were more accurate for the endpoints of the straight segments than for their midpoints. Because of this, only endpoints will be considered here; in other words, only even values of M will be considered. Wood and Li[8] found that the error in cases 2 and 3 was dominated by the "aligned segments" that begin or end immediately behind the control point. As shown in Fig. 1b, there are two aligned segments per revolution for case 3. This applies to case 2 as well, for different pairs of segments, but there are no aligned segments for case 1. Because the velocity induced by a straight segment on a control point must be normal to the plane containing the segment and the point, these segments make virtually no contribution to the binormal velocity at small pitch, whereas it is easy to see from the Biot–Savart integrand that they should make a major contribution if M is small. Using the solution from Ref. 4, Wood and Li[8] found that the accuracy of the straight-segment approximation is only $\mathcal{O}(M^{-1})$ at small M, (for example, around 10) improving to $\mathcal{O}(M^{-3})$ at very large M (for example $M \sim 300$). A crude estimate for the error was obtained from the trapezoidal rule applied to the section of the helix represented by the aligned segments. The dependence on M was reproduced, but the magnitude of the error was underestimated by a factor of about two. Many practical calculations use "moderate" values of M, that is, in the range 10–100. For example, the results in Fig. 1 of Bhagwat and Leishman[7] were obtained with $M = 36$. (In Ref. 8 a number of other issues relating to numerical accuracy of helical wake calculations are discussed that are not considered here.) It is, therefore, important to investigate the induced velocity errors further and, if possible, develop correction procedures for the significant errors that can occur when M is between 10 and 100. That is the purpose of the work described in this paper. Attention will be focused on small values of p that are typical of the wakes of wind turbines and rotors.

This paper begins by considering case 2 of Ref. 8 and significantly improves the error analysis therein. When the origin of the vortex angle in the Biot–Savart integrand (for the original helix) is changed to the junction between the aligned segments, the integrand is expanded in that angle and the resulting series integrated analytically for the first few terms. This procedure is equivalent to making a similarity transformation in which the similarity variable is the new angle divided by the index of the junction, which will be denoted by k: $k = 1$, 2, and 3 for the aligned segments identified in Fig. 1b. For small values of the similarity variable, the resulting estimates for the induced velocity are accurate to $\mathcal{O}(M^{-4})$, which is the same order as the curved segment expressions of Ref. 6. It is shown in the next section that the aligned segments are primarily responsible for the error in the binormal velocity at small and moderate values of M. An accurate correction is obtained by replacing the velocities induced by those segments with the similarity results.

The errors due to the aligned segments are likely to be greatest for constant radius helices, whereas the near wake consists of expanding or contracting vortices. A test case of an expanding helical vortex, for which the induced velocities are found using very accurate numerical quadrature, shows that corrections still need to be made only to the aligned segments. The following section describes some generic free-wake calculations of the wake of a three-bladed wind turbine operating near its design point, which demonstrate that replacement of the aligned segments is computationally efficient: The increase in execution time is significantly smaller than that required to give the same accuracy by increasing M without replacement.

Constant Radius Helical Vortices

Figure 1 shows a semi-infinite helical vortex, beginning at $(x, y, z) = (0, 1, 0)$ with constant pitch and radius. For the control point of case 2, U_b is given by

$$U_b = \frac{1}{(p^2+1)^{\frac{1}{2}}} \int_0^\infty \frac{-p^2\theta \sin\theta + (1-p^2)[1+\cos\theta]}{[p^2\theta^2 + 2(1+\cos\theta)]^{\frac{3}{2}}}\, \mathrm{d}\theta$$

$$= (p^2+1)^{\frac{1}{2}} W(\pi, p)/2 - p(p^2+1)^{-\frac{1}{2}} \qquad (1)$$

U_b is normalized by $\Gamma/(4\pi R)$ (as are all velocities in this paper), where Γ is the circulation and R is the vortex radius at $x = 0$. All lengths are normalized by R. The function $W(\pi, p)$, introduced by Ref. 4, can not, apparently, be determined analytically. It is given to six significant figures for $0.01 \le p \le 5.0$ in Table 1 of Ref. 8. These results were obtained using an adaptive quadrature scheme based on the Gauss–Kronrod method (for example, see Kahaner et al.[9], which was carefully checked to six significant figures against the asymptotic expansions for $W(\pi, p)$ at small and large pitch.[4] Wood and Li[8] point out that the accuracy could be easily extended to at least 10 significant figures, but the smaller number is sufficient for the present purposes.

One way to obtain an analytical approximation to the integral in Eq. (1) is to let $\theta' = \theta - k\pi$, where the index $k = 1, 3, 5, 7, \ldots$, so that $\theta' = 0$ defines the junction of the two aligned segments that occur for each revolution of the helix. Expanding the trigonometric functions and retaining all terms in θ' up to θ'^2 allows analytic integration to $\mathcal{O}(M^{-4})$ accuracy for small values of θ'. The indefinite form of Eq. (1) is thereby approximated as

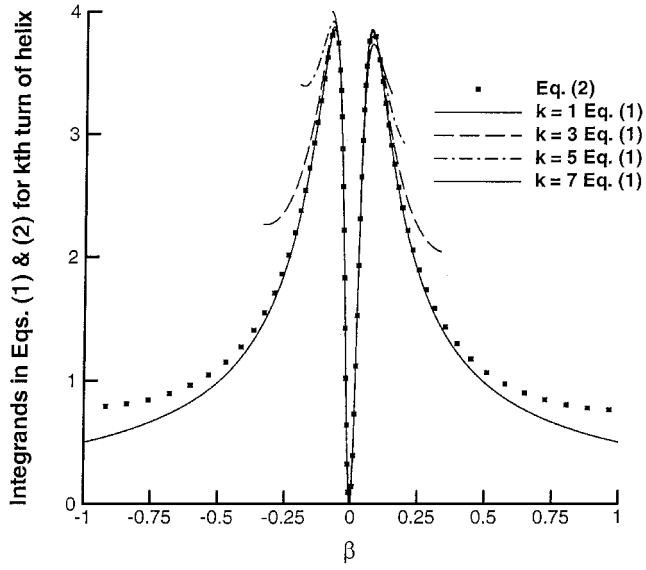

Fig. 2 Comparison of the exact Biot–Savart integrands for $k = 1, 3, 5,$ and 7 from Eq. (1) to the approximate integrand from Eq. (2); note that the integrands from Eq. (1) are scaled by $k\pi$ ($p = 0.05$).

$$\frac{1}{(p^2+1)^{\frac{1}{2}}}\int \frac{p^2\beta + \frac{1}{2}(1+p^2)\beta^2}{[p^2(1+\beta)^2+\beta^2]^{\frac{3}{2}}}\,\mathrm{d}\beta \tag{2}$$

where $\beta = \theta'/k\pi$. The integrand in Eq. (2) is shown in Fig. 2 to be a very accurate approximation to that in Eq. (1) for $k = 1, 3, 5,$ and 7, provided that β is small in magnitude. Because the integrand in Eq. (1) has its maximum at small $|\beta|$ (approximately $\beta = \pm\sqrt{2p}$ at small p) but is always zero at $\beta = 0$, the aligned segments should contribute significantly to the induced velocity for moderate M, but will make a negligible contribution when M is sufficiently large.

To use Eq. (2) to replace the induced velocity calculated from the aligned segments and their neighbors, let j be the vortex segment number counting from the junction of the aligned segments and note that, at the end of the jth segment, $\theta' = 2\pi j/M$ and $\beta_{j,k} = 2j/(kM)$. The integration of Eq. (2), as described in the Appendix, gives the contribution to the binormal velocity from the $2j$ segments surrounding the junction of the aligned segments as

$$\Delta U_{b,j,k} = \left\{p^2\left[F_1\left(p^2, \beta_{j,k}\right) - F_1\left(p^2, -\beta_{j,k}\right)\right] + (p^2+1)\left[F_2\left(p^2, \beta_{j,k}\right) - F_2\left(p^2, -\beta_{j,k}\right)\right]/2\right\}\Big/(p^2+1)^{\frac{1}{2}}$$

where

$$F_1(p^2, x) = \frac{1+x}{[p^2(1+x)^2+x^2]^{\frac{1}{2}}} \tag{3}$$

$$F_2(p^2, x) = \frac{p^2 - x + p^2x}{(1+p^2)[p^2(1+x)^2+x^2]^{\frac{1}{2}}} + \frac{1}{(1+p^2)^{\frac{3}{2}}} \times \log\left(2\left\{\frac{p^2+x+p^2x}{(1+p^2)^{\frac{1}{2}}} + [p^2(1+x)^2+x^2]^{\frac{1}{2}}\right\}\right)$$

The notation for F_1 and F_2 is explained in the Appendix. From Eq. (3), the contribution to the induced binormal velocity from all of the aligned segments is given by

$$\Delta U_{b,1} = \sum_{n=0}^{\infty} \frac{p^2\left[F_1\left(p^2, \beta_{1,2n+1}\right) - F_1\left(p^2, -\beta_{-1,2n+1}\right)\right] + (p^2+1)\left[F_2\left(p^2, \beta_{1,2n+1}\right) - F_2\left(p^2, -\beta_{-1,2n+1}\right)\right]/2}{(p^2+1)^{\frac{1}{2}}} \tag{4}$$

Because $\beta_{j,k}$ involves j as well as M, the stated order of accuracy $\mathcal{O}(M^{-4})$ is obtained only for small values of j. This restriction is also apparent from Fig. 2.

The basic notation for a straight segment is defined in Fig. 3. The contributions to U_s, V_s, and W_s, the x, y, and z velocities due to each segment, are given by Eq. (2) of Afjeh and Keith[10]:

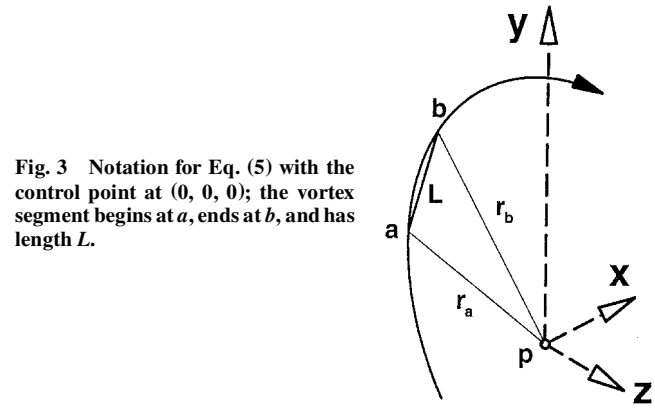

Fig. 3 Notation for Eq. (5) with the control point at (0, 0, 0); the vortex segment begins at a, ends at b, and has length L.

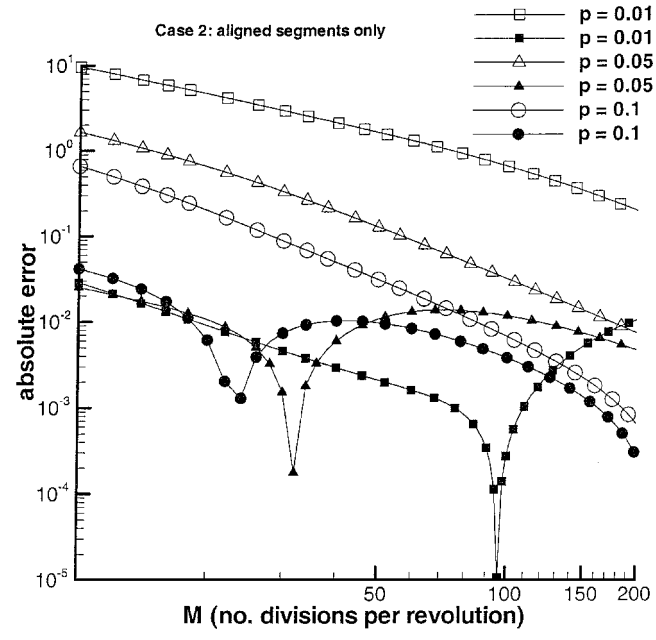

Fig. 4 Uncorrected (unfilled symbols) and corrected (filled symbols) straight-segment error for case 2 and values of pitch indicated; only the aligned segments are corrected.

$$\begin{bmatrix} U_s \\ V_s \\ W_s \end{bmatrix} = 2\frac{r_a + r_b}{r_a r_b\left[L^2 - (r_a+r_b)^2\right]} \times \begin{bmatrix} (y_p - y_b)(z_b - z_a) - (z_p - z_b)(y_b - y_a) \\ (z_p - z_b)(x_b - x_a) - (x_p - x_b)(z_b - z_a) \\ (x_p - x_b)(y_b - y_a) - (y_p - y_b)(x_b - x_a) \end{bmatrix} \tag{5}$$

Summing over all elements to obtain U, V, and W allows the binormal velocity to be calculated from

$$U_b = (U \pm pW)\big/(p^2+1)^{\frac{1}{2}} \tag{6}$$

where the plus sign is for case 2 and the minus for case 3. V will not be considered for the constant radius helix. Its determination, however, is required in the subsequent sections.

The open symbols in Fig. 4 show the magnitude of the uncorrected straight-segment error for case 2 and three values of p: 0.01, 0.05, and 0.1. The error is the difference between the straight-segment value and the "exact" value. These results are identical to those in Fig. 4b of Ref. 8 and are all negative. The M^{-1} dependence of the error at small M is most clearly seen for $p = 0.01$. The filled

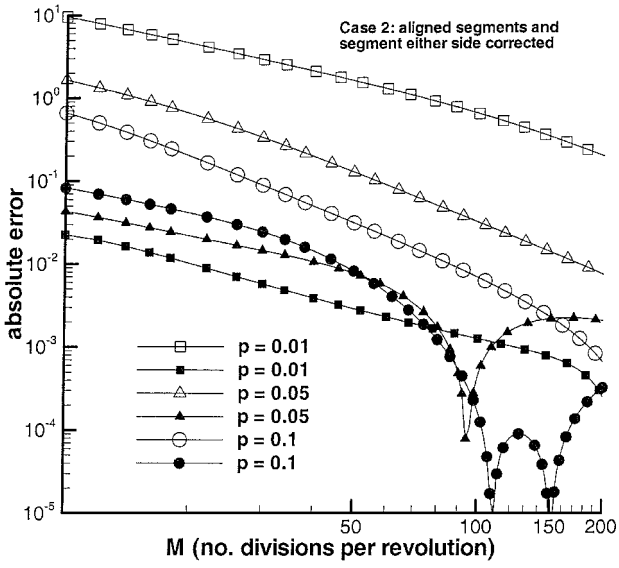

Fig. 5 Uncorrected (unfilled symbols) and corrected (filled symbols) straight-segment error for case 2 and values of pitch indicated; the aligned segments and segment either side are corrected.

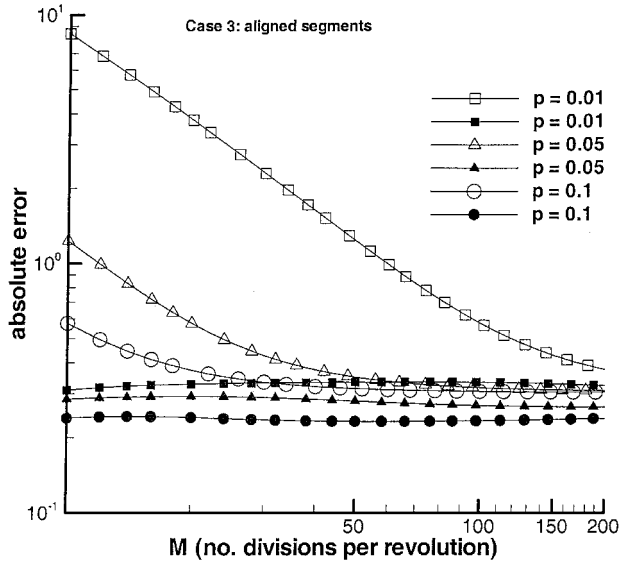

Fig. 6 Uncorrected (unfilled symbols) and corrected (filled symbols) straight-segment error for case 3 and values of pitch indicated; only the aligned segments are corrected.

symbols show the error when Eq. (4) is used instead of Eq. (5) to determine the contribution from the aligned segments. For small M, the error is positive but changes sign at a value of M that depends on p. The minimum error occurs at $M = M_{\min}$ near the change in sign; for $p = 0.01$, $M_{\min} = 96$, although errors of around 10^{-5} cannot be trusted. For $p = 0.05$, $M_{\min} = 32$, and for $p = 0.1$, $M_{\min} = 24$. The use of Eq. (4) for the aligned segments reduces the error by around two orders of magnitude for moderate values of M. As M increases further, the contribution to the velocity from the aligned segments decreases, and the new correction tends to zero. However, the corrected induced velocity is always more accurate than the uncorrected velocity. It is not apparent from Fig. 4 that the dominant contribution to the correction comes from the first pair of aligned segments, for which $k = 1$. For example, with $p = 0.05$ and $M = 30$, $\Delta U_{b,1}$ from Eq. (4) is 0.339261 and the contribution from $k = 1$ is 0.302671. If the segments on either side of the aligned segments are also replaced by the equivalent of Eq. (4), the error is as displayed in Fig. 5. The error was not significantly reduced from that shown in Fig. 4, indicating the dominant role of the aligned segments in producing the error.

For case 3, the self-induced velocity, the integral is the same as that in Eq. (1) but with the opposite sign for the trigonometric terms. From Ref. 8, the binormal velocity is given by

$$U_b = \frac{1}{(p^2+1)^{\frac{1}{2}}}\left[\frac{W(p)}{2} - p\right] + \frac{1}{2(p^2+1)}\left[\log 2 + 2p^2 - \frac{1}{2}\log(p^2+1)\right] \tag{7}$$

where $W(p)$, defined by Ref. 3, is also given to six significant figures in Table 1 of Ref. 8. Equation (7) does not include the curvature term, $\log(\varepsilon)/[2(1+p^2)]$, where $\varepsilon = a/(1+p^2)$ is the ratio of the core radius a to the vortex's radius of curvature. [See Eq. (5.7) of Ref. 4.] The curvature term arises from the need to exclude the region $|\theta| \le \varepsilon$ to avoid the θ^{-1} singularity in the Biot–Savart integrand at $\theta = 0$. It was omitted because straight segments cannot capture this curvature effect, and so the term would have to be added both to the straight segment result and to Eq. (7), leaving the error unchanged. However, the region $\varepsilon \le \theta \le 2\pi/M$, the rest of the first segment, should contribute $\log(2\pi/M)/[2(1+p^2)]$ to the order of accuracy of Eq. (3). Because a straight segment can not induce any velocity on itself, this amount was added to the binormal velocity calculated for all other segments using Eq. (5). Implementing the correction procedure is then a straightforward modification to that for case 2; Eq. (2) remains the same, except that now the index k takes on the values 2, 4, 6, ... Thus, no additional correction is made to the segment beginning at the control point. Figure 6 shows the resulting error for the uncorrected and corrected straight segments; the former were also shown in Fig. 5 of Ref. 8. The M^{-1} accuracy at small M is most obvious for $p = 0.01$. It is remarkable that the correction reduces the error to values that are nearly independent of M over its entire range. As pointed out by Wood and Li,[8] the magnitude of the error, around 0.3, is comparable to the effect on the induced velocity of the detailed structure of the vortex. For example, Ref. 3 proved that the binormal velocity for a helical vortex of zero thickness (and, hence, no structure) differs from that for a helical vortex with a finite circular core over which the vorticity is spread evenly, by one-quarter, for all values of p. This difference is ignored in the usual application of the Biot–Savart law and so does not appear in the corrections developed here. The structure of hovering rotor vortices has been measured in detail (for example, Ref. 5), but, to the author's knowledge, virtually nothing is known about the structure of vortex cores in the wakes of propellers and wind turbines. The effect of including the segments adjacent to the aligned segments is negligible, and so it is not shown.

Expanding Helical Vortices

The results from the preceding section indicate that the aligned segments are important because of their proximity to the control point. If the helix expands or contracts, as it must in the near wakes of propellers, rotors, and wind turbines, then the significance of the aligned segments will possibly change. Unfortunately, there are no analytical or asymptotic results available for expanding or contracting helical vortices, but an apparently useful test case has been constructed. Consider a conical helical vortex of constant pitch whose radius is given by $a\theta + 1$, where a is a constant, so that the radius is unity when $\theta = 0$, as is the case for the helix in Fig. 1. A typical value of a can be deduced from the hovering rotor experiments of Ref. 5, in which the trajectory of the tip vortex was determined and fitted by an empirical curve. The maximum contraction occurs at the blades and is approximately equal to $a = 0.035$. Because there are, apparently, no similarly detailed studies of wind-turbine wakes, this value will be used here for an expanding wake.

In any near-wake calculations, all three velocity components are required, but only the x-direction velocity U, and the y-direction V, will be considered. The Biot–Savart integrand for case 2 for U can be written as

$$\frac{(1-p^2)[a\theta + 1 + \cos\theta] + a\sin\theta}{[(p^2+a^2)\theta^2 + 2(a\theta+1)(1+\cos\theta)]^{\frac{3}{2}}} \tag{8}$$

The vortex consists of only five turns, which is sufficient to double the radius. Thus, $0 \le \theta \le 10\pi$. Using the adaptive Gauss–Kronrod quadrature method mentioned earlier, $U = 18.8777$ and $V = -14.4398$. The signs of these terms arise from Γ being

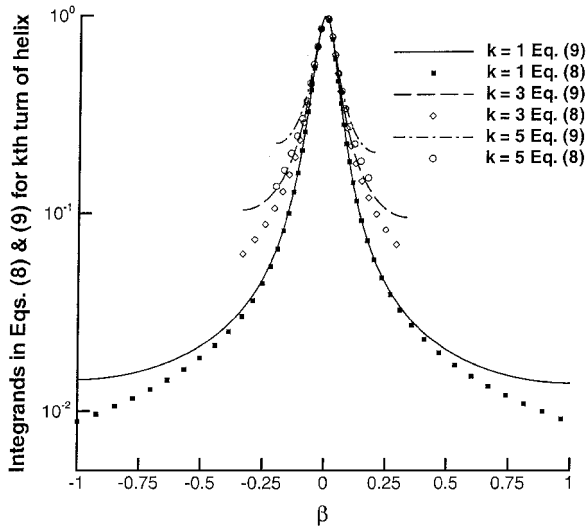

Fig. 7 Comparison of the exact Biot–Savart integrands for $k = 1$, 3, and 5 from Eq. (8) to the approximate integrand from Eq. (9); note that all integrands are scaled by their value at $\beta = 0$ and that the vertical axis is logarithmic ($p = 0.05$).

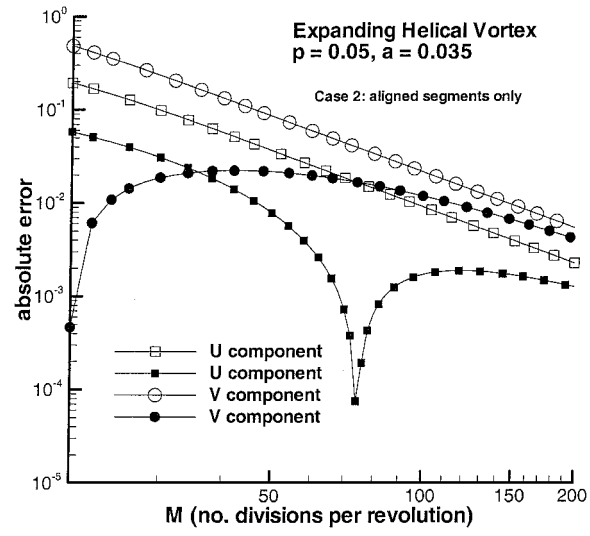

Fig. 8 Uncorrected (unfilled symbols) and corrected (filled symbols) straight-segment error for the expanding helical vortex; only the aligned segments are corrected.

taken as negative for wind turbines (expanding wakes), so that the Biot–Savart contribution will reduce the axial velocity below that of the wind, and the radial velocity will be positive. The calculations were done in double precision, and the estimated absolute error from the Gauss–Kronrod method for each integral was less than 4×10^{-10}. Thus, the values of U and V are likely to be accurate to at least the six significant figures used in Sec. II.

The transformation of Eq. (8) follows that of Eq. (2) and results in the approximate indefinite integral for U:

$$\frac{1}{k\pi(1+ak\pi)^{\frac{3}{2}}} \times \int \frac{a(1+ak\pi)+2a^2k\pi\beta+\frac{1}{2}(1+ak\pi+2a^2)\beta^2}{[\alpha(1+\beta)^2+\beta^2]^{\frac{3}{2}}}\,\mathrm{d}\beta \quad (9)$$

where $\alpha = (p^2+a^2)/(1+ak\pi)$. As for the earlier approximation (3), the integral is accurate to $\mathcal{O}(M^{-4})$ for small β. The integrand in Eq. (8) is compared to the full Biot–Savart integrand in Fig. 7 for $k = 1$, 3, and 5. Visually, the agreement is as good as that shown in Fig. 2, but the similarity is no longer exact because the approximate integrand is a function of k as well as β.

The contribution to the axial velocity from the $2j$ segments surrounding the junction of the aligned segments at each k is

$$\Delta U_{j,k} = \frac{1}{(1+ak\pi)^{\frac{1}{2}}}\left\{\frac{a}{k\pi}[F_0(\alpha,\beta_{j,k}) - F_0(\alpha,-\beta_{j,k})] + \frac{2a^2}{1+ak\pi}[F_1(\alpha,\beta_{j,k}) - F_1(\alpha,-\beta_{j,k})] + \left[\frac{1}{2}+\frac{a^2}{1+ak\pi}\right][F_2(\alpha,\beta_{j,k}) - F_2(\alpha,-\beta_{j,k})]\right\} \quad (10)$$

where

$$F_0(\alpha,x) = \frac{\alpha+x+\alpha x}{\alpha[\alpha(1+x)^2+x^2]^{\frac{1}{2}}}$$

and F_1 and F_2 are defined in Eq. (3). The corresponding contribution to the V component is

$$\Delta V_{j,k} = \frac{p}{(1+ak\pi)^{\frac{1}{2}}}\left\{-[F_0(\alpha,\beta_{j,k}) - F_0(\alpha,-\beta_{j,k})] - \frac{2a}{1+ak\pi}[F_1(\alpha,\beta_{j,k}) - F_1(\alpha,-\beta_{j,k}] + \left[\frac{k\pi}{2}-\frac{a}{1+ak\pi}\right] \times [F_2(\alpha,\beta_{j,k}) - F_2(\alpha,-\beta_{j,k})]\right\} \quad (11)$$

Figure 8 shows that the straight-segment calculation has errors in U and V that are $\mathcal{O}(M^{-2})$ over the range of M considered. Using Eqs. (10) and (11) significantly reduces the error, although the reduction is not as large as for the constant radius helix. The minimum error for U occurs at $M_{\min} = 74$ and that for V at $M_{\min} = 20$.

Application: Wind-Turbine Wakes

This section considers the computational effectiveness of the correction method outlined earlier. The corrections require additional execution time for any M, both in evaluating equations such as Eqs. (10) and (11) instead of Eq. (5), and in identifying the aligned segments in the first place. For any M, the correction will be effective only if the increase in accuracy can not be matched by increasing M (without correction) for the same execution time. In preparation for making this judgement, note that each iteration of a free-wake calculation without correction requires an execution time proportional to M^2.

The test case considered here is a generic model of a three-bladed wind turbine operating near its maximum efficiency, for which the velocity in the far wake U_∞ has the Lanchester–Betz value of $\frac{1}{3}$. Each blade is represented by a lifting line of strength Γ, and the shed vorticity resides in either the three tip vortices that expand in the near wake, or in the three hub vortices lying along the axis of rotation. By the use of a straightforward extension of the argument given by Wood[11] (see also Ref. 4), it is easy to show that

$$U_\infty = 1 - N\Gamma/(2\pi p_\infty) \quad (12)$$

where N is the number of blades and p_∞ is the pitch of the tip vortices in the far wake. All velocities are normalized by the wind speed and all lengths by the blade tip radius. Because

$$p_\infty \approx (1+U_\infty)/2\lambda \quad (13)$$

at sufficiently small pitch, where λ is the tip speed ratio,[4] it is possible to set Γ, once $N(=3)$ and λ have been chosen, to obtain a particular U_∞. For the calculations shown here, $\Gamma = 0.125$ and $\lambda = 7.5$, the latter being a typical design value for modern large wind turbines. The free-wake calculations were started from an initial wake of radius equal to the blade tip radius and pitch given by Eq. (13). Convergence was assumed when the root mean square of the radius of all segment endpoints changed by less than 10^{-7} between successive iterations. Typically, 30 iterations were required; this number hardly varied with M.

Equation (5) for each pair of aligned segments per revolution of each vortex was replaced by equations that are more complicated than for the special cases considered earlier. In terms of θ' introduced before Eq. (2), the integrands for the induced velocities at the control

Table 1 Coefficients of b_0, b_1, and b_2 in Eqs. (14) and (15)

Component	b_0	b_1	b_2
x	$(2a - r_0)\Delta r$	0	$(a^2 + \frac{1}{2}rr_0)\Delta r$
y	$(az/r + y)\Delta x$	$(ay/r - z)\Delta x + paz/r$	$p(ay/r - z) - \Delta x(az/r + y)/2$
z	$(ay/r + z)\Delta x$	$(az/r + y)\Delta x - pay/r$	$p(az/r + y) - \Delta x(ay/r - z)/2$

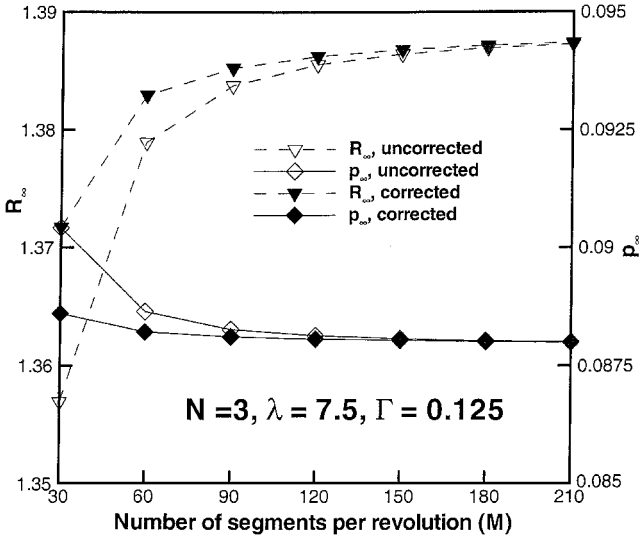

Fig. 9 Predicted far-wake radius and pitch for a three-bladed rotor.

point (x, y, z) due to the vortex passing through the junction of the aligned segments at (x_0, y_0, z_0) are of the form

$$\frac{b_0 + b_1\theta' + b_2\theta'^2}{\left[c_0 + c_1\theta' + c_2\theta'^2\right]^{\frac{3}{2}}} \tag{14a}$$

where, for all components,

$$c_0 = (\Delta x)^2 + (\Delta r)^2, \qquad c_1 = 2[p\Delta x + a\Delta r]$$
$$c_1 = 2\left[p^2 + a^2 + rr_0\right] \tag{14b}$$

In Eq. (14b) $\Delta x = x_0 - x$, and $\Delta r = r_0 - r$ is the difference in the radius of the two points. The coefficients in the numerator are given in Table 1 for the three velocity components. In general, $p = \mathrm{d}x/\mathrm{d}\theta$ and $a = \mathrm{d}r/\mathrm{d}\theta$. Both were evaluated at the junction using central differences.

The indefinite integral of Eq. (14) as determined by Mathematica is

$$G(b_0, b_1, b_2, x) = \frac{2\left[c_0c_1b_2 - 2b_1c_0c_2 + b_0c_1c_2 + \left(b_2c_1^2 - 2b_2c_0c_2 - b_1c_1c_2 + 2b_0c_2^2\right)x\right]}{c_2\left(4c_0c_2 - c_1^2\right)\left[c_0 + c_1x + c_2x^2\right]^{\frac{1}{2}}} + b_2\log\left[\frac{c_1 + c_2x}{c_2^{\frac{1}{2}}} + 2\left(c_0 + c_1x + c_2x^2\right)^{\frac{1}{2}}\right]c_2^{-\frac{3}{2}} \tag{15}$$

which was evaluated at $\theta' = \pm 2\pi/M$. The results for the far-wake radius, R_∞ and p_∞, are shown in Fig. 9 for $M = 210$, $U_\infty = 0.3217$, and $R_\infty = 1.3874$. The average velocity through the blades, $U_1 = U_\infty R_\infty^2 = 0.6192$, by conservation of mass, compares to $U_1 = (1 + U_\infty)/2 = 0.6609$ from the traditional one-dimensional wake analysis. A similar discrepancy occurs in the contracting wake of a hovering rotor; in both cases, it can be shown that the change in radius of the tip vortex accounts qualitatively for the change.[11]

Compared to the corrected values for $M = 210$, the changes in R_∞ and p_∞ for varying M are shown in Fig. 10. At the moderate value of $M = 30$, the "relative error" after employing Eq. (15) is comparable to that for the uncorrected results for twice the value of M. Employing the corrections at $M = 30$ increases the program's

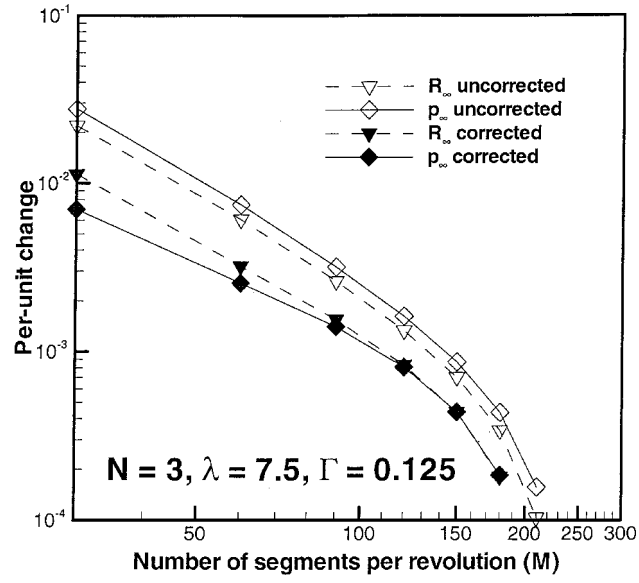

Fig. 10 Change in far-wake radius and pitch as M increases.

execution time per iteration by 60%, whereas doubling M causes a fourfold increase in time. Applying the corrections at $M = 60$ increased the run time by 30%, whereas M would have to increase to at least 90 to achieve a comparable error from the uncorrected calculations. This would cause an increase in execution time of over 200%. For both $M = 30$ and 60, at least half of the increase in applying the correction occurred in the identification of the aligned segments.

The errors shown in Fig. 10 for moderate values of M may be tolerable for some calculations, but there is at least one case where higher accuracy is essential. Wood[12] used the method described here to investigate generic wind-turbine wakes at high thrust and high levels of wake expansion. The success of the induced velocity calculations then becomes dependent on their ability to reproduce the higher-order terms in the binormal velocity[3,4] because the leading-order term, proportional to p^{-1}, is effectively canceled.

Conclusions

The straight-segment representation of helical vortices is computationally simple but can lead to significant errors in the induced velocity at the moderate values of the number of segments per revolution of the helix M used in many calculations. For the small values of the vortex pitch that typify the wakes of hovering rotors and wind turbines, the errors are caused largely by the pair of aligned segments for each revolution of the helix. The junction of these aligned segments is in line with the control point at which the velocity is required. The errors vary from M^{-1} at small M to M^{-2} at larger values. This paper develops a method to improve the accuracy of the induced velocities by ignoring the contribution from these segments in favor of expressions, derived from the Biot–Savart law for a helix, which are accurate to $\mathcal{O}(M^{-4})$. The expressions are applicable, however, only for segments close to the junction. As a consequence, the final level of accuracy of the induced velocity calculations is less than $\mathcal{O}(M^{-4})$. However, the corrections applied only to the aligned segments cause the total errors to change sign at small values of M, and so there is the possibility of judicially choosing M to minimize the error.

Two cases were considered for a constant pitch and radius vortex. Both control points were at the vortex radius, with the first (case 2) displaced by 180 deg from the beginning of the helix, and with

case 3 being the self-induced velocity. In both cases, the Biot–Savart integrand was zero at the junction of the aligned segments, but, as shown in Fig. 2, it quickly reaches a maximum on either side of the junction. Because the contribution to the induced velocity from the aligned segments is nearly zero at small pitch, the corrections should have a major effect at moderate values of M, but a negligible effect at sufficiently large M. The new expressions were found to reduce the error by around two orders of magnitude for moderate M. As expected, the reduction in the error tends to zero as M increases. The correction for the self-induced velocity is even more spectacular; Fig. 6 shows that the resulting error is almost independent of M and is comparable to the contribution to the vortex velocity from the structure of its core. At present, there is very little information available about the structure of helical vortices, except for those behind hovering rotors.

For the subsequent test case of an expanding vortex, the new method gave a significant improvement in accuracy, although the improvement was not as great as for the helix of constant radius.

A free-wake calculation of a three-bladed wind turbine operating near its design point was used to assess the effectiveness of the correction method for a typical application. For moderate values of M, the increase in accuracy due to the new method could be matched only by a significant increase in M without correction. This caused a much greater increase in execution time than did the extra calculations needed to implement the corrections.

In all cases, the use of the new corrections changed the sign of the error for small M from the uncorrected straight-segment errors. At sufficiently large M, the new corrections have a negligible effect. This suggests the possibility of adjusting M in a practical computation to minimize the error.

Appendix: Derivation of F_1, F_2, and F_3

These functions are the indefinite integrals defined by

$$F_n(\alpha, x) = \int x^n [\alpha(1+x)^2 + x^2]^{-\frac{3}{2}}\, dx$$

as determined by Mathematica. They arise from the expansion of the trigonometric functions in Eqs. (2) and (8) to $\mathcal{O}(\beta^2)$. To this level of approximation, the denominator in the expanding wake integral, Eq. (9), should read

$$(\alpha(1+\beta)^2 + \{1 + [ak\pi/(1+ak\pi)]\beta\}\beta^2)^{\frac{3}{2}}$$

The extra term in β^3 significantly complicates, and possibly prevents, analytical integration, and so it was omitted. This omission defines the order of truncation of the expansions of the trigonometric functions and leads to the statement in the main text that Eqs. (3), (10), and (11) are $\mathcal{O}(\beta^4)$ or $\mathcal{O}(M^{-4})$, provided that β is small.

Acknowledgment

This work was supported by the Australian Research Council.

References

[1]Ricca, R. L., "The Effect of Torsion on the Motion of a Helical Vortex Filament," *Journal of Fluid Mechanics*, Vol. 273, 1994, pp. 241–259.

[2]Kuibin, P. A., and Okulov, V. L., "Self-Induced Motion and Asymptotic Expansion of the Velocity Field in the Vicinity of a Helical Vortex Filament," *Physics of Fluids*, Vol. 10, No. 3, 1998, pp. 607–614.

[3]Boersma, J., and Wood, D. H., "On the Self-Induced Motion of a Helical Vortex," *Journal of Fluid Mechanics*, Vol. 384, 1999, pp. 263–280.

[4]Wood, D. H., and Boersma, J., "On the Motion of Multiple Helical Vortices," *Journal of Fluid Mechanics*, Vol. 447, 2001, pp. 149–171.

[5]Leishman, J. G., Baker, A., and Coyne, A., "Measurements of Rotor Tip Vortices Using Laser-Doppler Velocimetry," *Journal of the American Helicopter Society*, Vol. 41, No. 3, 1996, pp. 342–353.

[6]Bliss, D. B., Teske, M. E., and Quackenbush, T. R., "A New Methodology for Free Wake Analysis Using Curved Vortex Segments," NASA CR 3958, 1987.

[7]Bhagwat, M. J., and Leishman, J. G., "Stability Analysis of Helicopter Rotor Wakes in Axial Flight," *Journal of the American Helicopter Society*, Vol. 45, No. 1, 2000, pp. 165–178.

[8]Wood, D. H., and Li, D., "Assessment of the Accuracy of Representing a Helical Vortex by Straight Segments," *AIAA Journal*, Vol. 40, No. 4, 2002, pp. 647–651.

[9]Kahaner, D., Moler, C. B., and Nash, S., *Numerical Methods and Software*, Prentice–Hall, Upper Saddle River, NJ, 1989, pp. 153–155.

[10]Afjeh, A. A., and Keith, T. G., "A Simplified Free Wake Method for Horizontal-Axis Wind Turbine Performance Prediction," *Journal of Fluids Engineering*, Vol. 108, No. 4, 1986, pp. 400–406.

[11]Wood, D. H., "Effect of Tip Vortex Geometry on the Flow Through the Blades of a Hovering Rotor," *Journal of Aircraft*, Vol. 38, No. 3, 2001, pp. 583, 584.

[12]Wood, D. H., "Generic Vortex Modelling for Horizontal-Axis Wind Turbines," *Wind Engineering* (to be published).

R. M. C. So
Associate Editor